Dynamics and Chemistry of the Summer Stratosphere (DCOTSS)

Data Management Plan

Version 2.0

XX October 2021

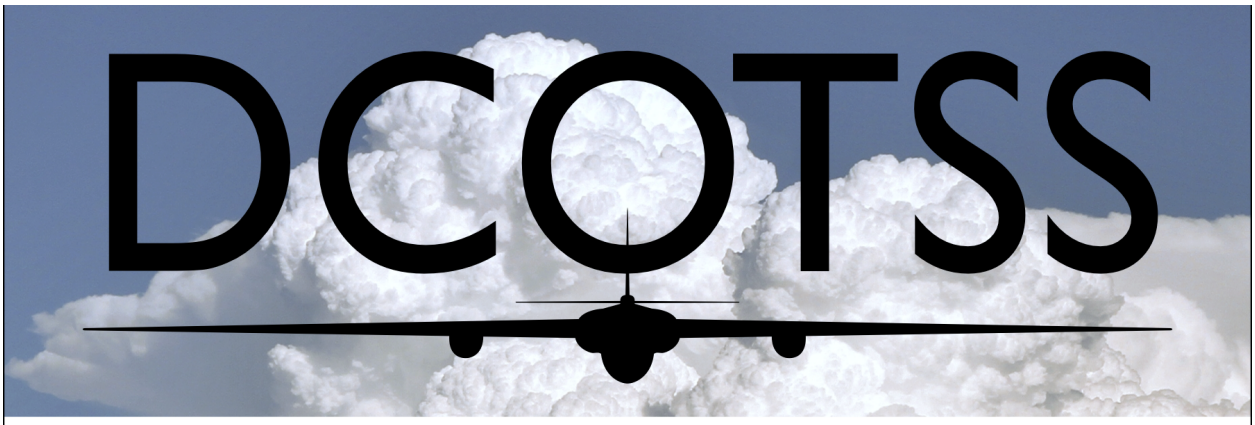

Prepared By:

Kenneth Bowman Principal Investigator	Date
Frank Kuetsch Deputy Principal Investigator	Date
Cameron Homeyer Data Manager and Science Investigation Manager	Date
David Sayres Investigator and Data Management Lead for Chemistry	Date

Change Log

Revision	Date	Description of Changes
V1.0	09-03-2019	Baseline Document
V2.0	12-01-2021	Complete Document

Table of Contents

1. Introduction

The Dynamics and Chemistry of the Summer Stratosphere (DCOTSS) mission investigates the role of tropopause-overshooting convection and the North American Monsoon Anticyclone (NAMA) in controlling the composition of the lower stratosphere above the conterminous United States. This Earth Venture Suborbital 3 (EVS-3) investigation will be executed in two phases with deployment of the high-altitude ER-2 aircraft in the summers of 2021 and 2022. In preparation for the first deployment, test flights were carried out in the spring of 2021 for instrument integration and performance evaluation. The following product types are produced by this investigation: airborne in situ chemical and meteorological measurements, remotely sensed observations (radar volumes, satellite imagery), numerical model output, and reports.

1.1. Purpose and Scope of the DMP

This Data Management Plan (DMP) identifies the data products that will be generated from the mission and describes the procedures and processes that will be used to ensure the transition of the data and associated information from the field to the Atmospheric Science Data Center (ASDC) where it will be archived and publicly available.

1.2. Parties Responsible for the DMP

The DCOTSS team is responsible for the development, maintenance, and management of this DMP. The Data Manager has overall responsibility for the plan, with all information and changes approved by the Principal Investigator (PI) and Deputy PI.

The DCOTSS Data Manager is Cameron Homeyer
University of Oklahoma, School of Meteorology
Email: chomeyer@ou.edu

The DCOTSS PI is Ken Bowman
Texas A&M University, Department of Atmospheric Sciences
Email: k-bowman@tamu.edu

The DCOTSS Deputy PI is Frank Kuetsch
Harvard University, School of Engineering and Applied Sciences
Email: keutsch@seas.harvard.edu

1.3. Summary of Data Processing Approach

Instrument PIs perform data processing and deliver airborne data products to the DCOTSS field archive for delivery to the ASDC. The DCOTSS forecasting and flight planning team performs data processing of remotely sensed observations and numerical model output and also delivers products to the DCOTSS field archive for delivery to the ASDC.

2. Investigation Overview

2.1. Investigation Summary

DCOTSS is a five-year mission funded as part of the Earth Venture Suborbital-3 program to enhance our understanding of tropopause-overshooting convection and the chemistry and meteorology of the lower stratosphere above the United States during summer. Strong convective storms are capable of rapidly transporting radiatively and chemically important atmospheric constituents from near the surface to the upper troposphere and lower stratosphere (UTLS). Tropospheric air can contain aerosols, water vapor, and trace gases, including halogen precursors implicated in possible stratospheric ozone loss. Once in the stratosphere, the large-scale NAMA circulation can both confine the convectively lofted air over the United States and extend its effects to intercontinental scales. However, the impact of tropopause-overshooting convection on the chemical composition of the LS, both within the monsoon anticyclones and in the broader global stratosphere, is poorly understood. Improving our understanding of tropopause-overshooting convection and its impact on the LS is the primary focus of DCOTSS. In addition to convection, DCOTSS will improve our understanding of the background chemical and thermodynamic state of the lower stratosphere against which the impact of large perturbations due either to natural or anthropogenic causes can be assessed. Fundamental science questions that DCOTSS will answer include:

1. How much tropospheric air and water is irreversibly injected into the stratosphere by convection?

2. Which convective source regions impact the NAMA?

3. What chemical changes take place in the stratosphere due to convection in the NAMA?

4. What is the background chemical and thermodynamic state of the LS over North America during summer?

The objectives of DCOTSS address two overarching science goals of the NASA Earth Science Research Program. Namely, DCOTSS will advance understanding of changes in the Earth's radiation balance, air quality and the ozone layer that result from changes in atmospheric composition and will improve the capability to predict weather and extreme weather events. DCOTSS will provide observations of convectively influenced air masses in the summertime LS that have not been targeted extensively in prior missions and these will help to develop an understanding of the impact of tropopause-overshooting convection on atmospheric composition and climate.

The NASA ER-2 is the airborne platform for DCOTSS, which offers ample payload space, weight capacity, power, and access to high altitudes (up to $\sim$21 km) necessary to achieve science goals. The flight endurance (8 hr) and range (3000 NM) of the ER-2 allow it to reach all regions of interest from the operations base in Salina, Kansas. Salina lies near the center of operational ground-based radar and geostationary satellite networks in the U.S. that will serve as key auxiliary data for the mission and within a region of frequent tropopause-overshooting convection during the months of May–August. The nominal deployment dates for DCOTSS are 7–17 June 2021 for testing (based out of Palmdale, California), and 12 July – 23 August 2021 and 10 May – 30 June 2022 for science. Up to eighteen (18) 6.5-hr research flights will be flown during each science

deployment, with approximately 8 flights targeting plumes in the LS 1-3 days downstream of their convective source, 2 survey flights to measure the background state of the LS, and 2 flights near ongoing convection.

The baseline payload aboard the ER-2 (illustrated in Figure 2.1) will provide:

- Continuous sampling of temperature, humidity, pressure, and winds.
- Continuous sampling of water vapor, ozone, and other chemically and radiatively important very short- to long-lived atmospheric trace gases.
- Continuous sampling of aerosol particles.
- Periodic sampling of air (up to 32 canisters per flight) that will be analyzed in a ground-based lab following each flight to determine the concentrations of an extensive set of trace gases with varying life times.

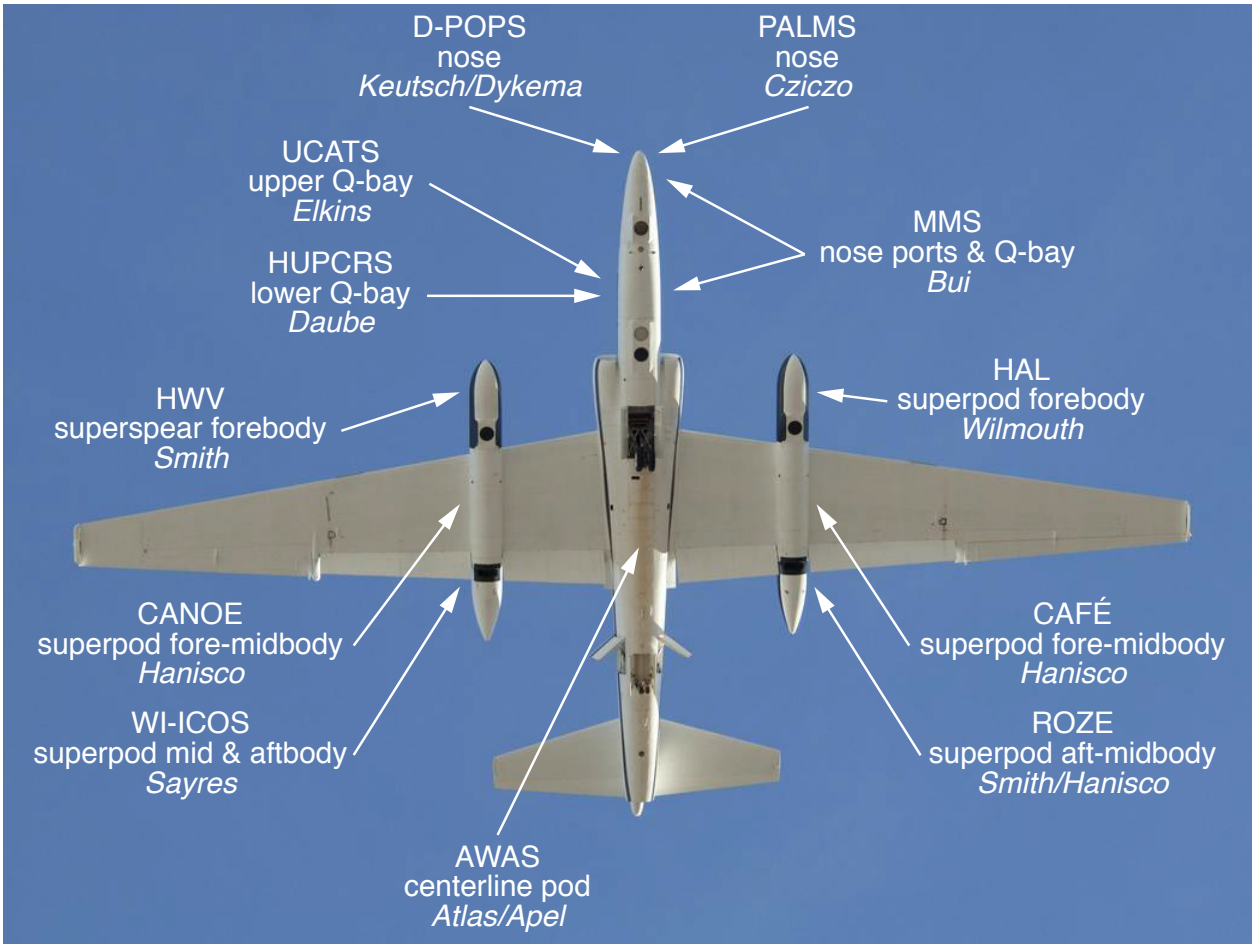

Figure 2.1: Baseline payload configuration for DCOTSS.

2.2. Investigation Instruments Summary Table

The NASA ER-2 is the sole platform for DCOTSS scientific instrumentation. The following subsections provide detailed overviews of each instrument. The locations of the instruments on the

ER-2 are illustrated in Figure 2.1 and a summary of the measurements they obtain is provided in Table 2.1.

Table 2.1: DCOTSS ER-2 payload.

Instrument	**Measurements**
Advanced Whole Air Sampler (AWAS)	>20 contituents with varying lifetimes
Compact Airborne Formaldehyde Experiment (CAFE)	Formaldehyde
Compact Airborne Nitrogen diOxide Experiment (CANOE)	Nitrogen Dioxide
Harvard Halogens (HAL)	Chlorine Monoxide, Chlorine Nitrate
Rapid OZone Experiment (ROZE)	Ozone
Harvard University Picarro Cavity Ringdown Spectrometer (HUPCRS)	Carbon Monoxide, Carbon Dioxide, Methane
Harvard Water Vapor (HWV)	Water Vapor
Meteorological Measurement Systems (MMS)	Pressure, Temperature, Horizontal and Vertical Wind
Particle Analysis by Laser Mass Spectrometry (PALMS)	Aerosol Composition
DCOTSS Printed Optical Particle Spectrometer (DPOPS)	Aerosol Size Distribution
UAS Chromatograph for Atmospheric Trace Species (UCATS)	Ozone, Water Vapor, Nitrous Oxide, Sulfur Hexafloride, CFC-11/12/113, Halon 1211/2402
Water Isotopologues – Integrated Cavity Output Spectrometer (WI–ICOS)	Water Vapor, Dueterated Water, Total Water (vapor + ice)

2.2.1. AWAS

AWAS consists of 32 canisters mounted in the centerline belly pod of the ER-2. The fill sequence of the canisters will be programmed to provide increased resolution during profiles and less frequent sampling during level legs by default. Remote control of sample collection from ground computers allows targeted sampling of specific features during flight (e.g., expected overshoot plumes). Following each flight, the onboard full AWAS canisters are replaced with a new set of canisters. Full canisters are analyzed with gas chromatography combined with mass spectrometry, flame ionization, and electron capture detectors. Mixing ratios of trace gases are calibrated against an in-house working standard that has been calibrated against primary standards and against other laboratories (1; 2; 3; 4).

Raw gas chromatographic data from the multiple detectors are evaluated using several software packages. The packages are: GCWerks (GC Soft), Chemstation (Agilent), and TERN (public access: https://sites.google.com/site/terninigor/home). The packages automatically integrate the peak area of each gas in the sample air and the standard gas to monitor detector response and drift

during the course of the analyses. Manual review and reintegration of peak areas is done as needed. The responsible co-Is for AWAS are E. Atlas (U. Miami) and E. Apel (NCAR).

2.2.2. CAFE

CAFE is an in situ instrument capable of measuring formaldehyde throughout the troposphere and LS (5). The instrument uses laser-induced fluorescence to obtain the high detection sensitivity and fast time response needed for airborne measurements. The fluorescence technique uses a new non-resonant detection that takes advantage of compact industrial lasers to minimize size and power requirements and enhance ruggedness and reliability. The instrument is designed for autonomous operation in flight and requires minimal support between flights. Air is pulled into the instrument, CH_2O molecules are excited by a UV laser, and the resulting fluorescence is measured by photomultiplier tubes. Time-gated counts are converted to pptv using a laboratory calibration. If the calibration is found to change, then reprocessing would be necessary. The responsible co-I for CAFE is J. St. Clair (NASA Goddard; Joint Systems for Earth Science Technology – JCET).

2.2.3. CANOE

CANOE is an in situ instrument capable of measuring nitrogen dioxide (NO_2) throughout the troposphere and LS (6). Except for the detectors, CANOE is a duplicate of CAFE and uses non-resonant laser-induced fluorescence. Air is pulled into the instrument, NO_2 molecules are excited by a green laser, and the resulting fluorescence is measured by photomultiplier tubes. Time-gated counts are converted to pptv using a laboratory calibration. If the calibration is found to change, then reprocessing would be necessary. The responsible co-I for CANOE is J. St. Clair (NASA Goddard; Joint Systems for Earth Science Technology – JCET).

2.2.4. HAL

The HAL instrument measures chlorine monoxide (ClO) and chlorine nitrate ($ClONO_2$) via atomic resonance fluorescence detection of Cl atoms in the vacuum ultraviolet. ClO is chemically converted to Cl via a rapid bimolecular reaction with NO, and $ClONO_2$ is thermally dissociated into ClO and NO_2, with the ClO fragments then detected in the same manner as ambient ClO.

HAL is calibrated in the laboratory under pressures and flow velocities typical of flight. The calibrations are run in nitrogen and air with different lamps and reaction distances. In flight, the absolute sensitivity of each detection axis is determined at systematic intervals from the observed Rayleigh scatter as a function of air density. The estimated accuracy is $\pm 17\%$ for the ClO measurements with a detection limit of 3 pptv. $ClONO_2$ is detected with an accuracy $\pm 21\%$ and a detection threshold of 10 pptv. ClO measurements are reported every 35 seconds, the length of the NO addition cycle, while $ClONO_2$ is reported less frequently due to the heater cycle (1000 seconds). Nonetheless, every reported measurement of $ClONO_2$ at the back axis represents an observation integrated over a 35-s time period, nearly concurrent (to within 10 s) with a simultaneous ClO measurement at the front axis. The responsible co-I for HAL is D. Wilmouth (Harvard U.).

2.2.5. ROZE

ROZE is a cavity-enhanced ultraviolet absorption instrument that detects in situ ozone (O_3). The instrument uses an LED light source at 265 nm that couples into an optical cavity generated by two high-reflectivity mirrors (R $>$ 99.7%). The light passes through the cell multiple times, creating an effective pathlength much larger than its physical footprint. O_3 is measured by direct absorption. Air is pulled into the sample cell via a 3-way solenoid valve that periodically directs the air flow through a MnO_2 scrubber to measure the baseline LED intensity in the absence of absorbing species or directly into the absorption cell to measure the intensity attenuated by any O3 within the sample. The instrument provides ambient mixing ratios of O3 at 1 Hz with a precision of 1 ppb and an accuracy of 6%. The responsible co-I for ROZE is J. Smith (Harvard U.).

2.2.6. HUPCRS

HUPCRS consists of a G2401-m Picarro gas analyzer (Picarro Inc., Santa Clara, CA, USA) repackaged in a temperature-controlled pressure vessel, a separate calibration system with 2 multi-species gas standards, and an external pump and pressure control assembly designed to allow operation at a wide range of altitudes. The Picarro analyzer uses Wavelength-Scanned Cavity Ringdown Spectroscopy (WS-CRDS) technology to make high precision measurements of greenhouse gases. HUPCRS reports concentrations of CO_2, CH_4, and CO every $\sim$2.2 seconds and the data are averaged to 10 seconds. The resulting in-flight precisions (accuracies) are CO_2: 20 (100) ppb, CH_4: 0.25 (1.0) ppb, and CO: 2.5 (3.5) ppb.

The sampling strategy for HUPCRS consists of bringing in air through a rear-facing inlet, filtered by a 2 μm Zefluor membrane, and dehydrating this air by flowing it through a multi-tube Nafion drier followed by a dry-ice cooled trap prior to entering the Picarro analyzer. A choked upstream Teflon-lined diaphragm pump delivers ambient air to the analyzer at 400 torr, regardless of aircraft altitude, via a flow bypass. A similar downstream pump, with an inlet pressure of 10 torr, facilitates flow through the analyzer at high altitude and ensures adequate purging of the Nafion drier. Measurement accuracy and stability are monitored by replacing ambient air with air from two NOAA-traceable gas standards (low- and high-span) for two minutes every 30 minutes. These standards are contained in 8.4 L carbon fiber wrapped aluminum cylinders and housed in a temperature-controlled enclosure. The responsible co-I for HUPCRS is B. Daube (Harvard U.).

2.2.7. HWV

The HWV instrument combines two independent techniques for the simultaneous in situ detection of ambient water vapor (H_2O) mixing ratios in a single duct: (1) the heritage Harvard Lyman-α photo-fragment fluorescence instrument (LyA) [Weinstock et al., 1994; Hintsa et al., 1999; Weinstock et al., 2009]; and (2) the Harvard Herriott Hygrometer (HHH), a tunable diode laser direct absorption instrument (7). Ambient mixing ratios of H_2O are recorded by each instrument at 1 Hz.

The simultaneous utilization of radically different measurement techniques facilitates the identification, diagnosis, and constraint of systematic errors both in the laboratory and in flight. As such, the combined instrument constitutes a significant step toward resolving controversies surrounding water vapor measurements in the upper troposphere and lower stratosphere. The responsible co-I for HWV is J. Smith (Harvard U.).

2.2.8. MMS

MMS provides calibrated, high-resolution measurements of ambient meteorological parameters (pressure, temperature, turbulence index, and the 3-dimensional wind vector) at 20 samples per second. MMS consists of three major systems: (1) an air motion sensing system to measure the air velocity with respect to the ER-2, (2) a motion sensing system to measure the ER-2 velocity with respect to the earth, and (3) a data acquisition system to process and record the measured quantities. The air motion sensing system consists of sensors, which measure temperature, pressures, and airflow angles (angle of attack and yaw angle). The Litton LN-100G and Systron Donner CMIGIT-III Embedded GPS Inertial Navigation Systems (INS) provide the aircraft attitude, position, velocity, and acceleration data. The Data Acquisition System samples the independent variables simultaneously and provides control over all system hardware. The responsible co-I for MMS is P. Bui (NASA Ames).

2.2.9. PALMS

The PALMS instrument is used to determine the chemical composition of aerosol particles on a particle by particle basis usage laser ablation mass spectrometry (LAMS). This type of instrument is typically called a single particle mass spectrometer (SPMS). PALMS focuses incoming particles using an aerodynamic inlet and a set of differential pumping stages. Particle detection and aerodynamic sizing occurs as particles pass through two 405 nm laser beams and scatter light. A 193 nm excimer laser is then triggered by a scattering event detected on the second laser beam and timed to strike the particle in the one step method that ablates and ionizes the components.

Particle vacuum aerodynamic diameter and chemical composition are measured in situ and in real time at the single particle level. In normal operating mode, sensitivity of the optical particle detection to scattered light sets the lower particle size limit to $\sim$150 nm. The ability to focus particles with the aerodynamic lens sets the upper particle size limit to $\sim$3000 nm. Particle data rate is set by the rep rate of the excimer laser and writing spectra to the computer; 20 Hz is possible although this is dependent on sufficient aerosol loading.

PALMS positive and negative spectra are acquired on a single particle basis in a format of signal generated versus mass/charge ratio. In practice LAMS spectra are all singly positively or negatively charged so the product is effectively signal versus ion mass. SPMSs are not considered to be quantitative on a single particle basis and precision is not typically given for a mass spectrum; spectra are signal versus mass. Data quality is determined as signal to noise ratio for each mass peak and all spectra with more than 1 peak over noise are archived. Signal to noise is therefore the quality of the data and it is reported for each mass spectra peak in each spectrum. Single particles are classified into broad compositional categories: sulfate-organic mixtures, biomass burning, elemental carbon, mineral dust, sea salt, meteoric, industrial, and oil combustion. Number fractions of these particle types are calculated over each time segment, and these averages are presented as the primary data products. If there were at least 5 suitable particles in a time interval, average values are calculated. The number of particles used to calculate the averages is also reported. The responsible co-I for PALMS is D. Cziczo (MIT/Purdue U.).

2.2.10. DPOPS

DPOPS is an in situ instrument capable of measuring particle number density as a function of size throughout the UTLS. The instrument uses a 405-nm diode laser to count and size individual particles (independent of composition and phase) in the size range 140–3000 nm. The instrument is designed for autonomous operation in flight and requires minimal support between flights. Though the instrument is commercially available (Handix Scientific, Boulder, CO), a custom inlet mounted in the free stream is needed to sample ambient air. The inlet design is platform dependent and designed to ensure fidelity of sampling with respect to size. The responsible co-I for POPS is J. Dykema (Harvard U.).

2.2.11. UCATS

UCATS is a combination of a three-channel NOAA custom gas chromatograph (GC), an ozone (O_3) absorption UV photometer (2B Technologies, Boulder, CO), and a dual-channel IR tunable diode laser (TDL) H_2O spectrometer, with different path lengths and absorption lines for different ranges of water vapor concentration (Port City Instruments, Reno, NV). The GC will measure nitrous oxide (N_2O) and sulfur hexafluoride (SF_6) every 70 seconds on channel 1; chlorofluorocarbons -11 (CCl_3F), -12 (CCl_2F_2), -113 ($CClF_2$-CCl_2F), and halon-1211 every 70 seconds on channel 2; and the compounds chloroform ($CHCl_3$), carbon tetrachloride (CCl_4), and short-lived perchloroethylene (PCE, C_2Cl_4) and trichloroethylene (TCE, C_2HCl_3) every 140 seconds on channel 3. Data quality is determined by calculating instrumental precision for each GC molecule using the reproducibility of the signal from periodic injections of standards. The responsible co-I for UCATS is J. Elkins (NOAA).

2.2.12. WI–ICOS

WI–ICOS measures water vapor and its major isotopologues using cavity enhanced absorption spectroscopy. Via an isokinetic inlet and heaters it measures total water (water vapor + ice). The primary measurement is an absorption spectrum. By fitting the absorption features along with measurements of pressure and temperature, mixing ratios of H_2O, HDO, $H_2^{18}O$ are produced at 1 Hz. It uses a continuous wave distributed feedback (cw-DFB) laser to scan across rotational-vibrational lines of H_2O and HDO in the mid-IR. Due to the low water vapor mixing ratios in the stratosphere, the absorption cell is composed of two highly-reflective mirrors that increase the effective pathlength by a factor of 2500. Ambient air is sampled by a side facing inlet that protrudes from the body of the superpod into free stream air. The instrument is periodically calibrated in flight using a system identical to that employed in the laboratory. All parameters used to calculate the mixing ratio of water vapor are calibrated before each campaign using NIST traceable standards. The responsible co-I for WI–ICOS is D. Sayres (Harvard U.).

3. Data Product Summary

3.1. Primary Data Product Details

The DCOTSS campaign will contain 12 primary instruments flown on the NASA ER-2. The primary data products from all in situ instruments are listed in Tables 3.1 to 3.6. Descriptions in §3.1.1 following the summary tables outline the data acquisition, data processing, data analysis, and data quality procedures used for each instrument. Tables 3.11 and 3.12 list the primary remote sensing data products, which will enable robust evaluation of the influence of recent convection on the observed air masses. Descriptions of data aquisition, processing, analysis, and quality for the remote sensing data are given after the tables in §3.1.2. Primary model data are listed in Table 3.13 and outlined in §3.1.3 and project reports are listed in Table 3.14 and outlined in §3.2. Common information for all instruments, such as time synchronization, transferal of data to the DAAC, file names and formatting are covered in §3.3.

3.1.1. Airborne Instrument Data

Table 3.1: Very short-lived (VSL) gas phase species (<1 month lifetime)

Data Product	Instrument	Sampling Interval	Precision ± Accuracy
Formaldehyde	CAFE	1 s	50 pptv ± 10%
Non-methane hydrocarbons	AWAS	variable*	<2-4 pptv ± 10%
Benzene, toluene	AWAS	variable*	2 pptv ± 10%
C_1-C_4 alkyl nitrates	AWAS	variable*	<1 pptv ± 20%
Chlorobenzene	AWAS	variable*	<0.1 pptv ± 20%
Methyl iodide	AWAS	variable*	<0.1 pptv ± 20%

*25–150 s depending on altitude

Table 3.2: Short-lived gas phase species (1 month to <1 year lifetime)

Data Product	Instrument	Sampling Interval	Precision ± Accuracy
Ethane	AWAS	variable*	<2 pptv ± 5%
1,2 dichloroethane	AWAS	variable*	<1 pptv ± 10%
Dichloromethane	AWAS	variable*	<1 pptv ± 10%
Chloroform	AWAS	variable*	<1 pptv ± 10%
Methyl Halides	AWAS	variable*	<0.1–0.5 pptv ± 10%
Solvents	AWAS	variable*	<0.1–0.5 pptv ± 10%
CO	HUPCRS	10 s	2.8 ppbv ± 3.5 ppbv

*25–150 s depending on altitude

Table 3.3: Long-lived gas phase species (>1 year lifetime)

Data Product	Instrument	Sampling Interval	Precision ± Accuracy
O_3†	ROZE	1 s	1 ppbv ± 6%
	UCATS	2 s	5 ppb ± 5%
H_2O	HWV	1 s	0.10 ppmv ± 10%
	UCATS	1 s	0.25 ppmv ± 10%
	WI–ICOS	10 s	0.25 ppmv ± 10%
δD	WI–ICOS	10 s	∼20‰ ± 40‰
CO_2	HUPCRS	10 s	20 ppbv ± 100 ppbv
CH_4	HUPCRS	10 s	0.2 ppbv ± 1 ppbv
N_2O	UCATS	70 s (3 s width)	1 ppbv ± 1%
SF_6	UCATS	70 s (3 s width)	0.05 pptv ± 1%
CFC-11/12/113	AWAS	variable*	<0.1–0.5 pptv ± 2%
	UCATS	70 s (3 s width)	1 pptv ± 1%
Halon 1211/2402	AWAS	variable*	<0.1 pptv ± 2%
	UCATS	70 s (3 s width)	0.05 pptv ± 1%
HCFC-141b/22/142b	AWAS	variable*	<1 pptv ± 2%
CCl_4	AWAS	variable*	0.5 pptv ± 2%
OCS	AWAS	variable*	3 pptv ± 5%
CH_3Cl	AWAS	variable*	3 pptv ± 5%

*25–150 s depending on altitude

†O_3 is utilized as a long-lived tracer. Its chemical lifetime is variable.

Table 3.4: Reactive and reservoir gas phase species

Data Product	Instrument	Sampling Interval	Precision ± Accuracy
ClO	HAL	35 s	3 pptv ± 17%
$ClONO_2$	HAL	35 s*	10 pptv ± 21%
NO_2	CANOE	1 s	40 pptv ± 10%

*varies with heater cycle

Table 3.5: Particles

Data Product	Instrument	Sampling Interval	Precision
Size Distribution	POPS	1 s	5% of diameter
Aerosol Composition	PALMS	up to 10 particles/s	N/A

Table 3.6: Meteorological data

Data Product	Instrument	Sampling Frequency	Precision ± Accuracy
Pressure	MMS	1–20 Hz	0.003 hPa ± 0.3 hPa
Temperature	MMS	1–20 Hz	0.05 K ± 0.3 K
Horizontal wind	MMS	1–20 Hz	0.1 m/s ± 1 m/s
Vertical wind	MMS	1–20 Hz	0.05 m/s ± 0.3 m/s

3.1.1.1. AWAS

Data Acquisition: Air samples are collected in stainless steel canisters during each flight for later analysis at the home institution of the PI. Analysis of the trace gas mixing ratios is performed with gas chromatography combined with mass spectrometry, flame ionization, and electron capture detectors. Mixing ratios of trace gases are calibrated against an in-house working standard that has been calibrated against primary standards and against other laboratories (1; 2; 3; 4).

Data Processing: Raw gas chromatographic data from the multiple detectors are evaluated using several software packages. The packages are: GCWerks (GC Soft), Chemstation (Agilent), and TERN (public access; https://sites.google.com/site/terninigor/home). The packages automatically integrate the peak area of each gas in the sample air and the standard gas to monitor detector response and drift during the course of the analyses. Manual review and reintegration of peak areas is done as needed.

Data will be submitted to the appropriate DAAC using the standard ICARTT file format that is common for NASA airborne measurements. Data version will be updated if changes are made to the reported measurements.

Data Analysis: Data is evaluated to identify potential outliers and artifacts through use of time series plots and tracer-tracer correlations. Questionable data will be flagged in the data file.

Data Quality: Data precision is assessed using replicate/duplicate analyses and calculations of standard variability. This information is included in the metadata for the AWAS instrument. Where possible, measurements of selected trace gases from AWAS will be compared to measurements from the UCATS instrument.

3.1.1.2. CAFE

Data Acquisition: CAFE measures CH_2O using a non-resonant laser-induced fluorescence technique. Air is pulled into the instrument, CH_2O molecules are excited by a pulsed 355 nm laser, and the resulting fluorescence (>420 nm) is measured by photomultiplier tubes. More instrumental detail is available in (5).

Data Processing: Data processing is performed in Matlab, taking in text files recorded by the instrument and outputting 1 Hz CH_2O data in ICARTT format. Time-gated PMT counts are converted to pptv using a laboratory calibration, following a fitting routine described in (5), where detailed information on data processing is available.

Data Analysis: As DCOTSS team members and others use the data, any issues with data quality will be assessed and acted upon by the CAFE team. If issues are identified, a further revision of the data will be produced.

Data Quality: If the data are of poor quality due to instrument issues, they will not be posted to the DAAC. All relevant data quality issues will be contained in the header of the data file.

3.1.1.3. CANOE

Data Acquisition: CANOE measures NO_2 using a non-resonant laser-induced fluorescence technique. Air is pulled into the instrument, NO_2 molecules are excited by a pulsed 532 nm laser, and the resulting fluorescence (>695 nm) is measured by PMTs. The instrument is nearly identical to the CAFE CH_2O instrument described in (5), with different PMT models and a different

wavelength laser.

Data Processing: Data processing is performed in Matlab, taking in text files recorded by the instrument and outputting 1 Hz NO_2 data in ICARTT format. Time-gated PMT counts are converted to pptv using a laboratory calibration, described with more detail in (6).

Data Analysis: As DCOTSS team members and others use the data, any issues with data quality will be assessed and acted upon by the CANOE team. If issues are identified, a further revision of the data will be produced.

Data Quality: If the data are of poor quality due to instrument issues, they will not be posted to the DAAC. All relevant data quality issues will be contained in the header of the data file.

3.1.1.4. HAL

Data Acquisition: The flow of ambient air through the Harvard Halogen instrument is controlled by a single primary bypass duct, 20-cm diameter, and twin nested secondary ducts, 5-cm square. The laminar core of the primary flow is extracted and decelerated to 10-15 m/s into the two mirror-image secondary ducts, where the ClO and $ClONO_2$ measurements are made. The nested-duct design not only aids in slowing the sample air but also in maintaining laminar flow and minimizing wall contact. The entrance to each secondary duct is a 26-cm long fairing. Just aft of the secondary duct inlets, nitric oxide (NO) injectors, consisting of nine perforated Teflon tubes, mix dilute NO (1:5 NO in N_2 along with nitrogen carrier gas) uniformly into the flow. An array of seven fast-response platinum resistance thermistors mounted on wire supports in each duct monitor the ambient air temperature immediately forward of the front detection axes, where Cl from the titration of ClO with NO is detected via ultraviolet resonance fluorescence. Each front detection axis is followed by a silicon strip dissociation heater. The heaters raise the air temperature in order to dissociate $ClONO_2$ prior to the rear detection axes, where the Cl atoms from $ClONO_2$ are measured. A second thermistor assembly downstream of the rear axis in each duct provides temperature data for the heated flow and allows feedback control of the dissociation heater. A pitot tube at the rear of the secondary duct reads ambient pressure and velocity, while a throttle valve near the secondary duct exit is used to control the flow velocity.

The fluorescence signals at the front detection axes are modulated primarily by the addition of NO, while the fluorescence signals at the rear detection axes are modulated by both NO addition and flow temperature. The typical mode of instrument operation involves a 35-second NO addition cycle consisting of four different flows followed by a null flow, where NO is off. The lowest two NO flow rates are chosen to optimize the conversion to Cl atoms for ClO, while the highest two flows optimize the conversion to Cl for $ClONO_2$. The NO addition cycle is synchronized with dissociation heater control algorithms of longer duration, which dither the temperature in one duct while scanning the temperature in the other.

The scanning mode of heater operation runs continuously over a 1000 second time interval, ramping the flow temperature up to 510 K in 26 K increments and back down in 50 K increments. Here the NO addition algorithm cycles two times per temperature step. The dither mode of heater operation steps between two different temperatures: 273 K, where no dissociation takes place and 510K, where $ClONO_2$ fully dissociates. At elevated temperature, the NO addition algorithm cycles three times. After every third dither cycle, the heater is shut off completely for 120 seconds. The dither mode is the primary method of heater operation, while the scanning mode provides critical diagnostic information regarding the temperature dependencies of the dissociation reactions.

Data Processing: The final data product is determined by applying the laboratory calibration to the observed signal, including a correction for any Lyman-α impurity in the RF lamp, and then applying the Cl yield for the conditions of the flight observation to obtain ClO or $ClONO_2$ concentration. All analysis is performed with MATLAB scripts. No ancillary measurements are required. ICARTT format will be used for the data submission.

Data Analysis: The instrument is calibrated in the laboratory under pressures and flow velocities typical of flight. The calibrations are run in nitrogen and air with different lamps and reaction distances. In flight, the absolute sensitivity of each detection axis is determined at systematic intervals from the observed Rayleigh scatter as a function of air density. The estimated accuracy is $\pm 17\%$ for the ClO measurements with a detection limit of 3 pptv. $ClONO_2$ is detected with an accuracy $\pm 21\%$ and a detection threshold of 10 pptv. ClO measurements are reported every 35 seconds, the length of the NO addition cycle, while $ClONO_2$ is reported less frequently due to the heater cycle. Nonetheless, every reported measurement of $ClONO_2$ at the back axis represents an observation integrated over a 35-s time period, nearly concurrent (to within 10 s) with a simultaneous ClO measurement at the front axis.

Data Quality: The primary indicator of data quality is the signal-to-noise ratio of the measurement. At times during DCOTSS, we may encounter ClO concentrations at or below the detection limit of the instrument. Beyond signal-to-noise, the quality of the data could be affected by instrumental issues such as: instability of an RF lamp, breakage of a silicon strip in the dissociation heater causing loss of a heating zone, or high / unstable Lyman-α impurity in a lamp. After every flight, all engineering data will be carefully examined for quality control and proper system function before the signal is processed into the final data product. If data are identified that are suspect, these can be excluded from the final data archive. The need to reprocess the submitted data and to resubmit final data could be triggered by a change to the laboratory calibration.

3.1.1.5. ROZE

Data Acquisition: ROZE measures O_3 via direct absorption in the deep ultraviolet utilizing a high-power LED light source with a centerline wavelength at 265 nm and a cavity-enhanced optical cell. The cell length is 30 cm, and the total absorption pathlength is $>$100 m as determined by calibration. Exiting light is passed to a photomultiplier tube (PMT) detector through a series of collection and filter optics.

Attenuation of light intensity in the optical cavity results from trace gas absorption as well as extinction due to the mirrors and Rayleigh scatter. Accounting for these additional losses, the Beer-Lambert absorption coefficient for O_3, α_{O_3}, is related to the observed change in intensity transmitted through the cavity as follows (8):

$$\alpha_{O_3} = \left(\frac{I_o - I}{I}\right)\left(\frac{1-R}{d} + \alpha_{Ray}\right) = \sigma_{O_3} N_{O_3} \tag{1}$$

Here, I_o is light intensity in the absence of any absorbing species, I is the intensity attenuated due to absorption, R is the mirror reflectivity, d is the physical distance separating the cavity mirrors, and α_{Ray} is the extinction due to Rayleigh scatter, a non-negligible component in the UV. The term $(1-R)/d$ gives the theoretical cavity loss, α_{cav}, and represents the inverse of the maximum effective optical pathlength. N_{O_3} is number density of O_3 and σ_{O_3} is the absorption cross section.

Accurate measurements require measurement of the I_o and I terms, knowledge of the Rayleigh and absorption cross sections in the detected spectral region, and calibration of the effective optical pathlength. Ambient air is pulled into the thermally regulated optical cell. A 3-way Teflon solenoid valve directs the flow alternately through a MnO2 scrubber assembly and into the absorption cell to measure I_o, or directly into the cell to measure I. Rayleigh scattering and absorption cross sections are taken from the literature (9; 10) and the pathlength is determined by regular calibrations either using attenuation as a function or pressure or known additions of O_3.

Data Processing: Raw I and I_o signals from the PMT are used to determine the number density of O_3 in the cell. Cell pressure and temperature data recorded by the flight computer are then used to convert O_3 number density to mixing ratio, the conserved quantity. All analysis is performed with MATLAB scripts that are available upon request.

Table 3.7: Data processing sequence for ROZE

ROZE Data Product	Level	Accuracy/Uncertainty	Resolution
Raw Detector Signal (Counts)	L0	N/A	10 Hz
Raw Pressure	L0	TBD	10 Hz
Raw Temperature	L0	TBD	10 Hz
ROZE Axis Pressure (hPa)	L1A	TBD	10 Hz
ROZE Axis Temperature (K)	L1A	TBD	10 Hz
O_3 Number Density (#/cc)	L1B	TBD	1 Hz
O_3 mixing ratio (ppmv)	L1B	TBD	1 Hz
O_3 mixing ratio + Unc. (ppmv)	L1B	TBD	1 Hz

Table 3.7 illustrates the data processing progression from the acquisition of raw data (Level 0) to archive data (Level 1B) that has undergone full quality assurance and quality control (QA/QC) and is ready for public dissemination through the DAAC. The levels are defined below:

- Level 0: Directly recorded quantities (spectra, counts, pressure, temperature) bearing original time tags in original format and resolution, archived with data acquisition software of corresponding version.
- Level 1A: Processed pressure and temperature data where minimal filtering and calibrations have been applied. Normalized signals, and time-referenced fitted spectra.
- Level 1B: Final O_3 mixing ratio data with accompanying uncertainties at 1 Hz. Final calibrations have been completed, QA/QC applied, and data archived using the standard ICARTT format.

*Note no ancillary measurements are required.

"Quick look" Level 1B data will be available usually within 24 hours of flight completion. Final Level 1B data will be available within 6 months of the end of each deployment. Level 0 data and the software necessary to analyze the raw data to produce the final product will only be available upon request.

Data Analysis: see (11)

Data Quality: The primary indicator of data quality is the signal-to-noise ratio of the measurement. Data quality may also be affected by a range of instrumental issues including drifts

or instability in the LED output power, drifts or instability in the detector sensitivity, and subtle changes in the optical alignment which can reduce power at the detector. Such changes may result from thermal or pressure effects in flight. An array of diagnostic data is routinely recorded and carefully examined post flight to evaluate instrument function and for data quality control. If data are identified to be suspect, they are excluded from the final data archive. The need to reprocess and resubmit final data would arise from a verifiable change to the instrument sensitivity identified through rigorous laboratory tests and calibration procedure.

3.1.1.6. HUPCRS

Data Acquisition: Briefly, the analyzer uses three distributed feedback (DFB) diode lasers in the spectral region of 1.55–1.65 μm. Monochromatic light is injected into a high-finesse optical cavity kept at 140 $\pm$ 0.1 Torr and 45 $\pm$ 0.02 °C by internal control elements and configured with three highly reflective mirrors (>99.995%). The light is blocked periodically and when blocked, the exponential decay rate of the light intensity is measured by a photodetector. The decay rate depends on loss mechanisms within the cavity such as mirror losses, light scattering, refraction, and absorption by a specific analyte. A sequence of specific wavelengths for each molecule is injected into the cavity in order to reconstruct the absorption spectra. High-altitude sampling (i.e., very low pressure and temperature) required transferring of the core components of the Picarro analyzer to a sealed tubular pressure vessel, which is maintained at 35 deg C and 1 atm. The analyzers components are isolated from the pressure vessel to provide vibration damping and decoupling from deformations in the pressure vessel caused by external pressure changes.

The sampling strategy for HUPCRS consists of bringing in air through a rear-facing inlet, filtered by a 2 μ Zefluor membrane, and dehydrating this air by flowing it through a multi-tube Nafion drier followed by a dry-ice cooled trap prior to entering the Picarro analyzer. A choked upstream Teflon-lined diaphragm pump delivers ambient air to the analyzer at 400 torr, regardless of aircraft altitude, via a flow bypass. A similar downstream pump, with an inlet pressure of 10 torr, facilitates flow through the analyzer at high altitude and ensures adequate purging of the Nafion drier. Measurement accuracy and stability are monitored by replacing ambient air with air from two NOAA-traceable gas standards (low- and high-span) for two minutes every 30 minutes. These standards are contained in 8.4 L carbon fiber wrapped aluminum cylinders and housed in a temperature-controlled enclosure. The total weight of the package is 195 lbs. (88.5 kg).

Data Processing: A fit to the spectra is performed in real time and concentrations are derived based on peak height. The final data product is produced by fitting and applying the flight calibrations to the raw collected data using MATLAB scripts. No ancillary measurements are required. ICARTT format will be used for the data submission.

Data Analysis: see (12)

Data Quality: One additional indicator of data quality beyond the instruments response to the flight standards is the species measurement interval. If the instrument is not successfully completing the expected number of ring-downs in the allotted time window for any of the 3 species, the measurement interval will become longer, indicating that something is wrong. By closely monitoring the recorded interval, the operator can identify data periods that are suspect, and exclude them from the final data. This occurs very infrequently.

The need to reprocess the submitted data and to resubmit final data can be triggered by a change to the primary calibration gas scale, which occasionally occurs. Changes of this nature are

generally due to NOAA refinements of their calibration procedures.

3.1.1.7. HWV

Data Acquisition: **LyA:** The Lyman-α photo-fragment fluorescence detection method was developed for the in situ measurement of stratospheric water vapor because of its molecular specificity and high sensitivity. Lyman-α radiation, generated by a small amount of hydrogen gas in a radiofrequency plasma discharge lamp, photo-dissociates water vapor in the sample duct. A fraction of the resulting OH fragments are formed in their first excited electronic state ($A^2\Sigma^+$) denoted OH*. These excited state fragments either fluoresce, or are quenched by collisions with nitrogen and oxygen. The OH* fluorescence at 315 nm is collected by a photomultiplier tube (PMT) positioned at right angles to the Lyman-α lamp.

$$S_{OH} = C_{flr} \cdot [H_2O] = \left(\frac{C_o}{1 + q_{air} \cdot [M]}\right) \rightarrow [H_2O] = S_{OH} \cdot \left(\frac{1 + q_{air} \cdot [M]}{C_o}\right) \tag{2}$$

Equation 2 shows that the signal detected by the PMT, SOH [photon counts], is directly proportional to the number density of water vapor in the detection volume of the instrument. The constant of proportionality, C_{flr} [(counts/s)/(molecules/cm^3)], is determined empirically, and implicitly includes terms related to the production of OH* via photo-dissociation, OH* fluorescence, as well as factors that determine the collection efficiency of the detection axis such as the transmissivity of the filter assembly in front of the PMT and the PMT quantum efficiency. A rearrangement of terms yields the two calibration constants of the detection axis: C_0, with units of [(counts/s)/(molecules/cm^3)], defines the sensitivity of the detection axis to [H_2O] at zero air density, and q_{air} [cm^3/molecule], is the empirically determined quenching factor in air with [M] equal to the number density of air. Because OH* fluorescence is strongly quenched by collisions at a rate proportional to the air density, at the altitudes of the upper troposphere and lower stratosphere, i.e., where $q_{air} \cdot [M] \gg 1$, the observed fluorescence signal is nearly proportional to the water vapor volume mixing ratio.

HHH: HHH measures water vapor via direct absorption in the near infrared utilizing a fiber-coupled tunable diode laser and a multi-pass Herriott cell. A fiber coupled 1.4 μm DFB laser is scanned over a strong water vapor absorption feature, in this case a single rotational-vibrational transition at 7178.75 cm^{-1}. The Herriott cell is comprised of two 3-inch mirrors, which are embedded in the walls (4 inches apart) of the primary duct of the HWV instrument. The cell supports a 92 pass pattern, generating a total absorption path of 10.05 m. The light intensity from each laser scan is detected by an InGaAs photodetector.

$$I = I_o \cdot e^{-\sigma \cdot l \cdot [H_2O]} \rightarrow [H_2O] = \left(\frac{1}{\sigma \cdot l}\right) \cdot ln\left(\frac{I_o}{I}\right) \tag{3}$$

The Beer-Lambert law, Equation 3, relates the transmitted light intensity of the laser, I, to the concentration of water vapor within the cell. The background, I_0, is determined through a polynomial fit to the baseline of the spectrum in regions outside of the water vapor absorption feature, the path-length, l, is determined by counting the number of passes through the cell and knowing the mirror separation, and the frequency dependent absorption cross-section, σ, is determined through simultaneous measurements of temperature and pressure within the HHH axis and spectral parameters from the HITRAN database.

Data Processing: **LyA:** In addition to raw photon counts from the PMT, a UV Diode positioned across the instrument duct from the LyA lamp records the LyA lamp flux. This is used to normalize the PMT signal in order to account for changes in LyA intensity in the detection volume. Empirically determined calibration coefficients are applied to raw pressure and temperature data recorded by the flight computer to yield accurate measurements of pressure and temperature within the LyA duct during flight. Finally, the empirically determined proportionality constants, C_0 and q_{air}, established during laboratory calibrations of the LyA instrument, are used in combination with duct temperature and pressure to convert the normalized PMT signal to measurements of ambient water vapor mixing ratio at 1 Hz. All analysis is performed with MATLAB scripts developed at Harvard. These scripts are available upon request. Details of the data processing and analysis routines, as well as the calibration procedure are contained in (13; 14; 15; 16).

Table 3.8: Data processing sequence for LyA

LyA Data Product	Level	Accuracy/Uncertainty	Resolution
Raw PMT Signal (Counts)	L0	N/A	4 Hz
Raw UV Diode Signal (Counts)	L0	N/A	4 Hz
Raw Pressure	L0	TBD	4 Hz
Raw Temperature	L0	TBD	4 Hz
Normalized Signal	L1A	N/A	4 Hz
LyA Axis Pressure (hPa)	L1A	TBD	4 Hz
LyA Axis Temperature (K)	L1A	TBD	4 Hz
H_2O Number Density (#/cc)	L1B	TBD	1 Hz
H_2O mixing ratio (ppmv)	L1B	TBD	1 Hz
H_2O mixing ratio + Unc. (ppmv)	L1B	TBD	1 Hz

HHH: The HWV data acquisition system includes a scalable signal processing (SSP) capability that averages the 52,600 points that comprise each individual spectral scan down to 1050 points. The SSP then coadds 799 of these averaged spectra to produce a single 1 Hz "raw" spectrum that is recorded by the flight computer for both the Herriott cell and etalon signals. These recorded scans are then processed using fitting algorithms designed at Harvard and written in the MATLAB technical programming language. The algorithms utilize a Voigt lineshape to represent the frequency dependent absorption cross-section, σ, and spectral parameters from the HITRAN database to calculate water vapor number density. Simultaneous measurements of temperature and pressure obtained within the HHH detection axis during flight are used to determine water vapor mixing ratio (ppmv) at 1 Hz. Details of the data processing and analysis routines, as well as the calibration procedure are contained in (16; 17; 7).

Tables 3.8 and 3.9 illustrate the data processing progression from the acquisition of raw data (Level 0) to archive data (Level 1B) that has undergone full quality assurance and quality control (QA/QC) and is ready for public dissemination through the DAAC. The levels are defined below:

- Level 0: Directly recorded quantities (spectra, counts, pressure, temperature) bearing original time tags in original format and resolution, archived with data acquisition software of corresponding version.
- Level 1A: Processed pressure and temperature data where minimal filtering and calibrations have been applied. Normalized signals, and time-referenced fitted spectra.

Table 3.9: Data processing sequence for HHH

LyA Data Product	Level	Accuracy/Uncertainty	Resolution
Raw HHH Spectra	L0	N/A	1 Hz
Raw Etalon Spectra	L0	N/A	1 Hz
Raw Pressure	L0	TBD	1 Hz
Raw Temperature	L0	TBD	1 Hz
HHH Axis Pressure (hPa)	L1A	TBD	1 Hz
HHH Axis Temperature (K)	L1A	TBD	1 Hz
H_2O Number Density (#/cc)	L1B	TBD	1 Hz
H_2O mixing ratio (ppmv)	L1B	TBD	1 Hz
H_2O mixing ratio + Unc. (ppmv)	L1B	TBD	1 Hz

- Level 1B: Final water vapor mixing ratio data with accompanying uncertainties at 1 Hz. Final calibrations have been completed, QA/QC applied, and data archived.

*Note no ancillary measurements are required.

Quick look Level 1B data will be available usually within 24 hours of flight completion. Final Level 1B data will be available within 6 months of the end of each deployment. Due to the volume and size of the original spectra, Level 0 data and the software necessary to analyze the raw data to produce the final product will only be available upon request.

Data Analysis: See (13; 14; 17; 15; 16; 7).

Data Quality: Calibrations are done in the laboratory before and after each campaign. Calibrations consist of water vapor addition at a variety of mixing ratios representative of the atmosphere. A variety of diagnostic temperatures, pressures, and voltages are recorded during flight to assess instrument health and to aid in QC/QA.

3.1.1.8. MMS

Data Acquisition: The MMS provides high-resolution and accurate meteorological parameters (pressure, temperature, turbulence index, and 3-dimensional wind vector). The basic wind derivation is the differencing of the aircraft ground velocity from the air velocity. The MMS payload consists of three major systems:

1. Air Motion Sensing System: contains sensors that measure static temperature, static and pitot pressure, and air incident angle with respect to the fuselage (to derive airflow angles such as angle of attack and yaw angle). Accurate measurements of these quantities require judicious choices of sensor locations, repeated laboratory calibrations, and proper corrections for compressibility, adiabatic heating, and flow distortion.

2. Inertial Navigation System (INS) with embedded GPS compensation: provides the aircraft attitude, position, velocity, and acceleration data.

3. Data Acquisition System: a multi-processor implementation which samples, processes and records the measured quantities. It consists of the CPUs, data storage units, communication and memory board, INS receiver, clock and terminal interfaces, analog-to-digital interfaces,

input/output interfaces, and power supplies. It also provides aircraft interfacing, over-all system hardware control, and real-time data computation and telemetry. The data acquisition software is highly customized to adapt the MMS to changing scientific needs.

Data Processing: The sampled 300 Hz raw data are first checked for time anomalies then desampled to 20 Hz engineering data. The measurements from the Air Motion System are used to determine the true airspeed with the application of appropriate sensor traceable calibration, aerodynamic flow correction (derived from induced aircraft maneuvers), and adiabatic compensation.

The groundspeed vector is derived from the integration of acceleration data using the appropriate numerical constraints and compensation. For example, the vertical acceleration data include compensation for distance above the surface, centrifugal, coriolis, and non-spherical Earth effects. The vertical integration is constrained by an altitude derived from the hydrostatic equation.

Data Analysis: The principal calibration is achieved from the analysis of in-flight induced maneuvers, which determine various angular offsets between the measurements, time-phase delays, flow distortion and aerodynamic compensation. For example, fundamental static pressure values depend on air speed, altitude, attitude and Reynolds number.

Data Quality: The primary data quality and performance verification is the requirement that the computed data products exhibit minimum perturbation induced by the aircraft motion during dedicated in-flight maneuvers. Power spectra of the measured quantities then validate the data resolution and noise figures. Final data are also compared with balloon sonde profiles, subject to availability.

3.1.1.9. PALMS

Data Acquisition: Particle vacuum aerodynamic diameter and chemical composition are measured in situ and in real time at the single particle level. In normal operating mode sensitivity of the optical particle detection to scattered light sets the lower particle size limit to $\sim$150 nm. The ability to focus particles with the aerodynamic lens sets the upper particle size limit to $\sim$3000 nm. Particle data rate is set by the rep rate of the excimer laser and writing spectra to the computer; $\sim$20 Hz is possible although this is dependent on sufficient aerosol loading.

Data Processing: Acquired PALMS NG positive and negative spectra are acquired on a single particle basis in a format of signal generated versus mass/charge ratio. In practice LAMS spectra are all singly positively or negatively charged so the product is effectively signal versus ion mass. SPMSs are not considered to be quantitative on a single particle basis and 'precision' is not typically given for a mass spectrum; spectra are signal versus mass. PALMS aerosol size for each spectrum for diameter $\sim$150 to $>$3000 nm (typically the PALMS size range spans the peak of the aerosol mass mode).

Single particles are classified into the particle types shown below. Number fractions of these particle types are calculated over each time segment, and these averages are presented as the primary data products. If there were at least 5 suitable particles in a time interval, average values are calculated. The number of particles used to calculate the averages is also reported. Other data products, including size-resolved composition, are available - contact the PI.

- Positive ion mode data products: SulfOrgNitFrac, BioBurnFrac, SootFrac, MineralFrac, MeteoricFrac, AlkaliSaltFrac, SeaSaltFrac, OilCombFrac, UnclassFrac

The Sulfate/Organic/Nitrate fraction (0 to 1) is the number fraction of particles that are identified as sulfate/organic/nitrate internal mixtures. Likewise for particles identified as biomass burning, soot, mineral dust/metallic, meteoric, alkali salts, sea salt, heavy oil combustion (vanadium tracer), and unclassified (other) particles.

- Negative ion mode data products: OrgSulfMF

  OrgSulfMF is the mass fraction of organic material relative to sulfate: Org mass/(org+sulf mass) = 0–1. This parameter is a calibrated quantity and is only calculated for particles that are sulfate-organic-nitrate internal mixtures (which is often the predominant particle type).

Data Analysis: PALMS NG is calibrated for mass spectral peaks and aerosol size both prior to and post mission. Standard reference materials (e.g. polystyrene latex spheres of known size and composition) are used for calibration and to set uncertainty in size measurements. Spectral peaks are defined as ion mass.

Data Quality: Data quality is determined as signal to noise ratio for each mass peak and all spectra with more than 1 peak over noise are archived. Signal to noise is therefore the 'quality' of the data and it is reported for each mass spectra peak in each spectrum. PALMS NG data are not typically reprocessed unless a systematic instrument issue is resolved after the initial data processing (this is extremely unlikely).

3.1.1.10. DPOPS

Data Acquisition: Instrument acquires intensity of scattered light from single particles transiting its 405 nm laser beam. Size range for particles is 140 nm - 3000 nm diameter. This size range is divided into 100 volume-doubling size bins. Particles per size bin are logged at 1 Hz intervals.

Data Processing: Scattered light intensity is converted into particle size based on the theoretical refractive index of the aerosols, the particle shape, and standard scattering theory. Uncertainty due to deviation from nominal refractive index and particle shape will be calculated and archived as part of the data product. Uncertainty due to scattering amplitude precision and Mie resonances will also be included.

Data Analysis: Instrument will be calibrated by measuring a known size distribution of calibration particles (18).

Data Quality: The flight data will be qualified based on housekeeping data to ensure the gas flow rate and number density of particles is within the operating range of DPOPS (73 particles per cm^3 at nominal operating volumetric flow of 1.7 L min^{-1}).

3.1.1.11. UCATS

Data Acquisition: UCATS is a combination of a three-channel NOAA custom gas chromatograph (GC), an ozone (O_3) absorption UV photometer (2B Technologies, Boulder, CO), and a dual-channel IR tunable diode laser (TDL) water vapor (H_2O) spectrometer, with different path lengths and absorption lines for different ranges of H_2O concentration (Port City Instruments, Reno, NV). The GC will measure nitrous oxide (N_2O) and sulfur hexafluoride (SF_6) every 70 seconds on channel 1; chlorofluorocarbons -11 (CCl3F), -12 (CCl2F2), -113 (CClF2-CCl2F), and halon-1211 every 70 seconds on channel 2; and the compounds chloroform (CHCl3), carbon tetrachloride (CCl4),

and short-lived perchloroethylene (PCE, C2Cl4) and trichloroethylene (TCE, C2HCl3) every 140 seconds on channel 3.

Data Processing: Step by Step Methods:

1. Preflight: The GC needs to run the day before each flight for a couple of hours or more. On the day of the flight, we will need crew support to load the instrument in the upper Q-bay. We also have the ECD detectors warmed up to maximum temperature (350 °C) before the flight for ∼1 hr. We monitor the signal of the detectors, pressures on gas cylinders, housekeeping during the warm-up process on the ground in the hangar to evaluate the health of the instrument.

2. During flight: We monitor the real time data stream for engineering (ECD temperature, N_2 carrier gas pressures, and detector signals) and mixing ratios of O_3 and H_2O, along with values for the strongest signals from the GC (N_2O, SF_6, CFCs, CCl_4). If there is a problem, then the only action that we can take is to restart the instrument which reboots our data system and controllers.

3. Post flight: We retrieve the flash card from the instrument and download the instrument into the lab and warm up the instrument to inspect the health of the instrument. We have someone attend the post flight briefing with pilots and management. We report our instrument status based on real time data analysis and our estimate of the health of the instrument. The GC channel data are processed with our custom GC software and preliminary ICARTT files are created. The H_2O and O_3 files have preliminary calibrations applied and we create preliminary ICARTT files for distribution to the team and project management.

We will attempt to have final data archived in 6 months, but a more realistic estimate is 9 months after the deployment based on adding new channel and performance during ATom.

Data Analysis: We run a full suite of GC standards in the lab for the GC before and after the deployment. We bring a calibrated water vapor standard and run it during the deployment. We calibrate the ozone instrument in the lab before and after each deployment, but can also bring a calibration source of ozone to run in the field.

Data Quality: Data quality is determined by calculating instrumental precision for each GC molecule using the reproducibility of the signal from periodic injections our standards. We report errors for each trace gas mixing ratio based on precision of the signal from the in-flight calibration standard and the goodness of fit for calibration curves obtained on the ground. N_2O is in parts-per-billion by mole fraction (ppb), and other GC gases in parts-per-trillion by mole fraction (ppt). Atmospheric O_3 is measured with a precision of 5 ppb and 2 second frequency and H_2O with a precision of 0.25 parts-per-million (ppm) at 1 Hz for stratospheric water ($<$10 ppm).

We plan to send down in real time some of the GC data, O_3, and H_2O. Lab calibrations in the field and home base (Boulder) are critical. All GC data are reprocessed after each flight; O_3 often only needs some QA/QC before final data are produced. H_2O will require the application of calibrations during the beginning and end of each deployment.

3.1.1.12. WI–ICOS

Data Acquisition: The water isotopes instrument is an absorption instrument that uses highly reflective mirrors to increase the effective pathlength of the optical detection cell. A distributed

feedback (DFB) laser is tuned over several absorption features in the 2.65 μm region of the spectrum. These spectra are digitized at 100 MHz, average to 1 MHz, with a single spectra containing approximately 2000 points. This results in 500 spectra bring recorded each second. These spectra are then co-added to produce 1 spectra each second which is recorded on a flash drive. Along with the spectra, pressure and temperature in the cell are recorded at 1 Hz which is necessary to calculate the number density in the cell used to produce volume mixing ratios.

Air is drawn into a forward facing inlet. Isokinetic flow is maintained by measuring the pressure outside and inside the inlet and driving the pressure difference to zero via a throttle valve near the exhaust. The valve is controlled using a PID loop. Air from the inlet is picked off and directed into the main detection axis with flow being maintained by a oiless dry scroll pump.

Data Processing: Table 3.10 illustrates how the data obtained by the various measurements is used to derive products and which instruments/teams are needed for each derived product. The data processing will take place at different levels outlined below.

Table 3.10: Data processing sequence for WI–ICOS

WI–ICOS Data Product	Level	Accuracy/Uncertainty	Resolution
Raw Spectra	L0	N/A	1 Hz
Raw Etalon Spectra	L0	N/A	1 Hz
Raw Pressure	L0	TBD	1 Hz
Raw Temperature	L0	TBD	1 Hz
Cell Pressure (hPa)	L1A	TBD	1 Hz
Cell Temperature (K)	L1A	TBD	1 Hz
H_2O mixing ratio (ppmv)	L1B	0.1 ppmv 10%	1 Hz
H_2 ^{18}O mixing ratio (ppmv)	L1B	5.0 ppbv 10%	1 Hz
HDO mixing ratio (ppmv)	L1B	0.4 ppbv 10%	1 Hz
δD	L2	$20‰ \pm 40‰$	1 Hz
$\delta^{18}O$	L2	$20‰ \pm 40‰$	1 Hz
Ice Water Content (IWC)	L2	0.2 ppmv 15%	1 Hz

- Level 0: Data as directly measured quantities (spectra, pressure, temperature) and bearing original time tags in original format at full original resolution archived with processing software of corresponding version.
- Level 1: Processed and fitted spectra to produce concentrations at full original resolution, de-spiked and time-referenced, containing calibration coefficients and ancillary information.
- Level 2: Processed Output Data: Derived geophysical and chemical variables at the same resolution as Level 1, including some variables derived from multiple measurements. Quality checked.
- Level 3: Any averaged data, profiles, reprocessed data for model inputs or other products produced using the Level 2 data as needed for publications.

Quick look Level 1 data will be available usually within 24 hours of a flight. Full Level 1 data will be available within 3 months of the end of each year of campaigns. Level 2 data will

be available and archived within 6 months of the end of each year of campaign. Level 3 will be available and archived as produced. Due to the volume and size of the original spectra, Level 0 data will be available upon request along with the software necessary to analyze the raw spectra to produce concentration. The software is open-source (written at Harvard). Data formats and metadata standards will follow NASA ESDIS standards as described in Standards, Requirements and References. All data will be archived using the ICARTT format.

Data Analysis: Details of data analysis and fitting routines are contained within (17)

Data Quality: Calibrations are done in the laboratory before and after each campaign as well as during each flight. Calibrations consist of water vapor addition at a variety of mixing ratios representative of the atmosphere. A variety of diagnostic temperatures, pressures, and voltages are recorded for purposed of assessing instrument health and to aid in QC/QA.

3.1.2. Remotely Sensed Data

Two remotely sensed datasets are generated in near-real-time for forecasting and flight planning purposes during each science deployment and reprocessed into final versions for archival in the 6 months following deployment: GridRad data and overshoot identifications from GOES imagery. Details on the archived products for these datasets are given in Tables 3.11 and 3.12, respectively.

Table 3.11: Radar data

Data Product	Spatial Resolution	Frequency
Radar Reflectivity	$\sim$0.02° × 0.02° × 0.5–1 km longitude-latitude-altitude	10 min
Spectrum Width	$\sim$0.02° × 0.02° × 0.5–1 km longitude-latitude-altitude	10 min
Echo Top Altitude	$\sim$0.02° × 0.02° longitude-latitude	10 min
Overshooting Tops	$\sim$0.02° × 0.02° longitude-latitude	10 min

Table 3.12: Satellite data

Data Product	Horizontal Resolution	Frequency
Cloud Top Altitude	2 km	10 min
Overshooting Tops	2 km	10 min
Visible Texture Rating	2 km	10 min

3.1.2.1. Gridded NEXRAD WSR-88D Radar (GridRad) Data

GridRad data (19) will be produced at 10-min frequency across the contiguous United States (CONUS) to support forecasting and flight planning activities for DCOTSS. These data will also enable analyses linking storm characteristics to the in situ measurements collected aboard the ER-2. GridRad data include volumes of radar reflectivity at horizontal polarization (providing information on the size and/or concentration of precipitation particles within a storm) and radial velocity spectrum width (providing information on storm kinematics, including turbulence). The volumes have 0.5-km vertical grid spacing from 0.5-7 km altitude above sea level (ASL) and 1-km vertical grid spacing above 7 km (up to 22 km ASL). The primary utility of these data will be identifying tropopause-overshooting convection (echo tops above the environmental tropopause altitude) over the CONUS. Overshoots will be linked to aircraft observations using air trajectory calculations, which will also be archived (described in §3.1.3). Identifying overshoots requires tropopause altitude information, which will be provided by operational weather forecast models for forecasting during DCOTSS deployments and by atmospheric renalyses (e.g., MERRA-2) for the overshoot identifications that will be archived at the ASDC.

Though produced in near-real-time during the mission, GridRad data will be reprocessed following each deployment using the final NEXRAD data archive available. The accuracy of echo top altitudes from GridRad is well documented, with negligible bias and an uncertainty of ± 1 km (e.g., 20; 21; 22). Accuracy of the radar reflectivity and velocity spectrum width measurements has been well documented for NEXRAD WSR-88D radars (23; 24).

GridRad data will be archived in netCDF-4 format, with internal compression to minimize storage requirements. Due to the large-area, high-resolution grids, volume data will also be written in "sparse" format, where only volumes containing echo will be written to the file along with their three-dimensional locations on the full analysis grid. This approach is consistent with the public hourly archive of GridRad data that exists for years 1995–2017 (19). The 10-min GridRad volume files range in size from ∼75 to ∼130 MB. GridRad volumes will be archived for the entirety of each deployment, including a week prior to the flight period. For the two science deployments, this amounts to an approximate total of 1.5 TB of GridRad data that will be archived. The responsible co-Is are C. Homeyer (U. Oklahoma) and K. Bowman (Texas A&M).

3.1.2.2. Satellite Data

Tropopause-overshooting convection will also be identified using GOES visible (VIS) and infrared (IR) geostationary satellite imagery for DCOTSS using a method outlined in (25; 26). Products that will be archived include derived cloud top altitude, convective overshoot probability, and VIS texture rating product (a measure of the 'bumpiness' of a cloud top and a skillful indicator of an overshoot). Satellite products will be produced in near-real-time using GOES-16 and -17 imagery at 10-minute intervals. The product domain will extend over North America and encompass most of Mexico and Canada. The overshoot products from satellite will complement those provided by GridRad and will uniquely enable an understanding of overshooting that occurs outside of the coverage of the NEXRAD radar network (e.g., over the ocean, Canada, and the Sierra Madre Occidental in Mexico). The satellite-based products will also enable identification of cloud-top signatures of stratospheric injection such as above-anvil cirrus plumes (VIS and IR evidence of the injection of ice particles into the stratosphere). Such physical evidence of convective injection of cloud material (and likely, tropospheric air) into the stratosphere is not provided by alternative data sources. If developed during the time period of the DCOTSS mission, objective identifications of above-anvil cirrus plumes may also be archived.

All satellite data products will be archived at the ASDC in netCDF-4 format. Similar to GridRad data, satellite products will be archived for the entirety of each deployment, including a week prior to the flight period. Thus, the anticipated total storage required for satellite data is ∼1 TB. The responsible co-I is K. Bedka (NASA Langley).

3.1.3. Numerical Model Output

Model output will be archived as created following each deployment. Two primary datasets will be produces: 1) trajectory forecasts initialized at tropopause-overshooting convection locationas and along each DCOTSS flight path, and 2) convection-allowing model simulations for select flights. These are summarized in Table 3.13.

3.1.3.1. Air Trajectory Calculations

Air parcel trajectories will be computed for DCOTSS using the TRAJ3D trajectory model (27; 28; 29). TRAJ3D is flexible and allows the use of different vertical coordinates, horizontal domains (global or regional), and wind inputs. Trajectory calculations will be computed using large-scale isentropic wind fields from global operational models for forecasting and from reanaly-

Table 3.13: Model output

Data Product	Temporal Resolution	Frequency
Overshoot Trajectories	1 hr	Initialized every 10 min
Flight Trajectories	1 hr	Initialized every second
Convection Allowing Model Output	5 min – 1 hr	Select Flights
Chemistry Model Output	10–60 s	All Flights

sis output for archival. Two types of trajectory products will be created and archived at the ASDC: flight trajectories and overshoot trajectories. Flight trajectories will be initialized every second along each DCOTSS flight track (one file per initialization) and run backwards for up to 10 days. Overshoot trajectories will be initialized in overshoot volumes identified from both GridRad and satellite data every 10 minutes (one file per initialization time) and run forward for up to 5 days. These trajectory calculations will be stored in netCDF-4 format and particle positions will be written every hour along a trajectory's path. The total estimated size of archived trajectory calculations is expected not to exceed 200 GB. The responsible co-Is are C. Homeyer (U. Oklahoma) and K. Bowman (Texas A&M).

3.1.3.2. Convection Allowing Model Output

To both aid in the evaluation of aircraft observations and evaluate the ability of numerical models to represent overshooting convection and transport, convection allowing model simulations will be performed for select DCOTSS flights. These simulations will be carried out using the Weather Research and Forecasting model (30) coupled with Chemistry (31; 32) – WRF-Chem.

Based on prior grid resolution and physical/chemical parameterization sensitivity studies for the representation of overshooting convection (33; 34), the planned model design for DCOTSS simulations is as follows: Simulations will be run with one-way nesting from a parent domain encompassing North America with a horizontal grid spacing of 12.5 km to a nested domain with 2.5-km spacing that is large enough to include any convection and convective outflow sampled by the ER-2. The vertical grid will consist of more than 100 levels with a nominal grid spacing of 250 m in the free troposphere and stratosphere and a model top of 10 hPa ($\sim$30 km). A 5-km deep damping layer will be employed to prevent reflection of spurious waves off the model top. Meteorological initial and boundary conditions will be provided every 3-6 hours by a state-of-the-art reanalysis system or forecast model. Chemical initial and boundary conditions will be defined using output from the Model of Ozone and Related chemical Tracers, version 4 (MOZART-4; 35). Parameterizations selected include the microphysics parameterization (NSSL 2-moment; (36)), planetary boundary layer scheme (Yonsei University; (37)), and chemical mechanism (Regional Atmospheric Chemistry Model; (38; 39)) coupled with the Modal Aerosol Dynamics Model for Europe/Secondary Organic Aerosol Model (MADE/SORGAM; (40; 41)). In addition, Smagorinsky first-order closure will be used for horizontal subgrid-scale mixing and the RRTMG scheme will be used for both short-wave and long-wave radiation (42). Anthropogenic emissions will be generated using the latest National Emissions Inventory data provided by the Environmental Protection Agency. Biogenic emissions will be calculated online with the Model of Emissions of Gases and Aerosols from Nature (MEGAN V2.04; (43)). Finally, photolysis rates will be calcu-

lated using the Fast-J scheme (44; 32).

For each flight selected for WRF-Chem simulation, the parent domain will be initialized and run using meteorology only (i.e., no chemical trace gas and aerosol processes). The simulated meteorological fields will then be downscaled to the nested domain (Δx = 2.5-km) and run with full chemistry. Both parent and nested domains will be initialized 6-12 hours before the occurrence of convection and run until the conclusion of the DCOTSS flight. Output will retained from the nested domain every 5-60 minutes, depending on the scientific goal of the simulations for each case.

In addition to predicted meteorological and chemical fields, each simulation will likely include passive tracers to aid in the tracking of convectively influenced air over time. The design of passive tracer packages included in the simulations may vary depending on the scientific goals of each case. Regardless of model design, the format for convection allowing model simulation output will be netCDF-4 (one file per time) and the expected data volume of DCOTSS simulations is up to $\sim$3 TB. The exact size of the data volume will depend on model design and the number of cases simulated, which is not known at this time. The responsible co-Is will be C. Homeyer (U. Oklahoma) and G. Mullendore (NCAR).

3.1.3.3. Chemistry Model Output

Photodissociation frequencies (J values) will be computed for DCOTSS using a radiative transfer model of the ultraviolet and visible (UV/Vis) spectral regions (45). It is planned that J values for 105 species (some species repeated using various cross sections) will be provided as well as other radiative transfer quantities of interest, at the temporal resolution, along each DCOTSS flight track, matched to the time interval of the 10 second merge files. The J values are found by constraining profiles of ozone to total column ozone and reflectivity in the UV/Vis region to satellite mesaurements. This product has been used in many prior ER-2 based campaigns (46; 47; 48); the list of species include radical and reservoir compounds in the nitrogen, hydrogen, chlorine, bromine and iodine families. J values for additional species can be provided upon request.

Output of a photochemical steady state (PSS) model chemical box model (49) constrained by DCOTSS direct measurements of temperature, pressure, aerosol surface area, ozone, water vapor, methane, nitrous oxide and DCOTSS-specific tracer-tracer relations for NOy, Cly, and Bry will also be provided. The model output will be for radical and reservoir compounds in the nitrogen, hydrogen, chlorine and bromine. This model product has been used in many prior ER-2 based campaigns (48; 50). Currently we plan to provide PSS results every minute along the flight track of each DCOTSS flight; PSS results at 10 sec resolution will be provided for interesting flight segments such as cold, wet, convectively injected plumes.

3.2. Associated Data Products to be Archived

Day-to-day operations in the field during each science deployment will involve daily forecasting and flight planning meetings and written reports of each mission (flight) conducted. Several products summarizing these activities will be archived at the ASDC, summarized in Table 3.14 and outlined below.

Table 3.14: Project reports.

Data Product	Temporal Resolution	Frequency
Mission Summaries	N/A	1 per flight
Pilot reports	N/A	1 per flight
ER-2 Navigational Data	N/A	1 per flight
Forecasting and Flight Planning Briefings	N/A	Daily

3.2.1. Aircraft flight reports

After each flight, the ER-2 pilot and mission management team will submit a flight report through the Airborne Science Program (ASP) Website on-line system. This is a requirement of the ASP management for all SMD aircraft flights. The report will be automatically linked to the DCOTSS archive at the ASDC.

3.2.2. Mission scientist reports

Two types of reports will be produced by the mission scientists. Daily reports will provide high-level summaries of daily weather conditions and forecasts and the flight tasking decisions and options for the ER-2 for the current and next several days. This will be posted and archived and available to all DCOTSS participants.

Science flight summary reports by the mission scientists will be produced after each flight. This report will (for each flight) provide a summary of instrument operating status, the forecasting and planning sequence leading into the mission, and a description of significant events that occurred including problems related to the aircraft or instruments, weather conditions during flight and key observations related to the mission science objectives. This will also be submitted through the ASP Website online system and will be combined with the flight report to create one document accessible through the DCOTSS website calendar.

3.2.3. Forecaster reports

Forecasting and flight planning briefings will be prepared on a daily basis during each deployment. The briefings will include information on local conditions at Salina, current conditions for the larger NAMA region, the likelihood of tropopause-overshooting storm formation, and the history and trajectory forecasts for recent observed tropopause-overshooting storms. Forecasters will prepare briefings each day (excluding down days) during deployments, usually in the form of PowerPoint presentations. These summaries will be archived in PowerPoint or PDF format.

3.2.4. ER-2 navigational data

Navigation data from all ER-2 flights will be archived at the ASDC.

3.3. Data Acquisition, Distribution and Archiving

Each instrument team is responsible for their own data acquisition and processing with details for each instrument described in section 3.1. In general each instrument contains a hard drive or

flash drive that records raw data during the flight. At the end of each flight this data is transferred to instrument team computers via ethernet or USB for analysis and initial archiving on the field archive maintained by ESPO. Many instruments produce 'quick look' data made available within 24 hours. Though lacking rigorous QA/QC it is nevertheless useful for initial assessment of flight goals and is used for subsequent flight planning.

The field archive is updated by individual instrument teams as they are able to further process their data with final products expected at or before six months after the end of each summer's final science campaign. At that point the ESPO field archive is updated with final data and that data will be transferred to the ASDC via standard secure internet protocols and data transmission checked via file check sums such as MD5 or similar.

All DCOTSS data products will conform to industry standards. All instrument computers will be time-synchronized to the NPTD server on the ER-2. In cases where time synchronization is not possible or fails, MMS will be used as a reference time for other instruments. All instruments teams will archive using the ICARTT format, with one file per flight. Merge files of multiple instruments will be archived in netCDF-4 format, also one file per flight. Where available, ATBDs will be provided to the ASDC for distribution with the data products. Science software used to produce the products will be provided to the ASDC at the end of the investigation with the final products. Proprietary software is excluded from this requirement. File and variable names, design, and data volume are listed in Table 3.15.

All data will be finalized and submitted to the ASDC within six months after the end of each summer's science mission(s) unless either: (1) data issues are identified and the product requires reprocessing, or (2) processing requires longer than six months. In cases of reprocessing, the instrument Co-I will process the data and deliver to the ASDC for distribution with updated documentation and software. The Co-I will notify the ASDC to inform them of the need for re-delivery and give a time frame of when to expect the data. A summary of the anticipated collection and ASDC delivery dates is provided in Table 3.16.

3.4. Expectations for the Distributed Active Archive Center

The DCOTSS team expects the ASDC to provide convenient, cite-able, and easily navigable public access to mission data sets. This includes the ability to quickly identify and access DCOTSS data and metadata through web searches, digital object identifiers (DOIs), and searches via the ASDC system. All data access and information should be available within 1 month of transfer of DCOTSS data to the ASDC and the ASDC should help the DCOTSS team ensure deadlines for data submission and access are met.

Table 3.15: File definitions, variable names, and expected file size for in situ data products. All file names will have a date appended to them in the format _YYMMDD to represent the date data was taken. Each file is for one flight.

Instrument/PI	**File Name**	**Product(s)**	**Variable Name(s)**	**Independent Variable**	**Data Volume**
AWAS/Atlas/Apel	AWAS		Time		10 MB
CAFE/Hanisco	CAFE	CH2O	Gas_CH2O_InSitu_S_AVMR	Time	1 MB
CANOE/Hanisco	CANOE	NO2	Gas_NO2_InSitu_S_AVMR	Time	1 MB
HAL/Wilmouth	HAL	ClO ClONO2	Gas_ClO_InSitu_S_AVMR Gas_ClONO2_InSitu_S_AVMR	Time	1 MB
HOZ/Smith	HOZ	Ozone	Gas_O3_InSitu_S_AVMR	Time	1 MB
HUPCRS/Daube	HUPCRS	CO CO2 CH4	Gas_CO_InSitu_S_AVMR Gas_CO2_InSitu_S_AVMR Gas_CH4_InSitu_S_AVMR	Time	1 MB
HWV/Smith	HWV	Water Vapor	Gas_H2O_InSitu_S_AVMR	Time	1 MB
MMS/Bui	MMS	Pressure Temperature Horizontal Wind Speed Vertical Wind Speed	Met_StaticPressure_InSitu Met_StaticAirTemperature_InSitu Met_WindSpeed_InSitu Met_WWindSpeed_InSitu	Time	1 MB
PALMS/Czisco	PALMS	Aerosol Composition	TBD	Time	TBD
POPS/Keutch/Dykema	POPS	Size Distribution	TBD	Time	TBD
UCATS/Elkins	UCATS_O3 UCATS_H2O UCATS_MS	Ozone Water Vapor N2O SF6 CFC11 CFC12 CFC113 H1211 chloroform CCl4 C2Cl4 C2HCl3	Gas_O3_InSitu_S_AVMR Gas_H2O_InSitu_S_AVMR Gas_N2O_InSitu_S_AVMR Gas_SF6_InSitu_S_AVMR Gas_CFC11_InSitu_S_AVMR Gas_CFC12_InSitu_S_AVMR Gas_CFC113_InSitu_S_AVMR Gas_H1211_InSitu_S_AVMR Gas_CHCl3_InSitu_S_AVMR Gas_CCl4_InSitu_S_AVMR Gas_C2Cl4_InSitu_S_AVMR Gas_C2HCl3_InSitu_S_AVMR	Time Time Time	1 MB 1 MB 10 MB
WI–ICOS/Sayres	WIICOS	Total Water (Vapor + Ice) D/H ratio of H2O	Gas_H2O_InSitu_S_TW Gas_H2O_InSitu_S_dD	Time	1 MB

Table 3.16: Data collection and ASDC delivery dates.

Deployment	**Deployment end date**	**Data submission deadline**
1	23 August 2021	28 February 2022
2	30 June 2022	31 December 2022

4. References

[1] S. M. Schauffler, E. L. Atlas, D. R. Blake, F. Flocke, R. A. Lueb, J. M. Lee-Taylor, V. Stroud, and W. Travnicek, "Distributions of brominated organic compounds in the troposphere and lower stratosphere," *J. Geophys. Res.*, vol. 104, no. D17, pp. 21,513–21,535, 1999.

[2] F. Flocke, R. L. Herman, R. J. Salawich, E. Atlas, C. R. Webster, S. M. Schauffler, R. A. Lueb, R. D. May, E. J. Moyer, K. H. Rosenlof, D. C. Scott, D. R. Blake, and T. P. Bui, "An examination of chemistry and transport processes in the tropical lower stratosphere using observations of long-lived and short-lived compounds obtained during STRAT and POLARIS," *J. Geophys. Res.*, vol. 104, no. D21, pp. 26,625–26,642, 1999.

[3] B. D. Hall, A. Engel, J. Mühle, J. W. Elkins, F. Artuso, E. Atlas, M. Aydin, D. Blake, E.-G. Brunke, S. Chiavarini, P. J. Fraser, J. Happell, P. B. Krummel, I. Levin, M. Loewenstein, M. Maione, S. A. Montzka, S. O'Doherty, S. Reimann, G. Rhoderick, E. S. Saltzmann, H. E. Scheel, L. P. Steele, M. K. Vollmer, R. F. Weiss, D. Worthy, and Y. Yokouchi, "Results from the international halocarbons in air comparison experiment (IHALACE)," *Atmos. Meas. Tech.*, vol. 7, pp. 469–490, 2014.

[4] S. J. Andrews, L. J. Carpenter, E. C. Apel, E. Atlas, V. Donets, J. R. Hopkins, R. S. Hornbrook, A. C. Lewis, R. T. Lidster, R. Lueb, J. Minaeian, M. Navarro, S. Punjabi, D. Riemer, and S. Schauffler, "A comparison of very short lived halocarbon (VSLS) and DMS aircraft measurements in the tropical west Pacific from CAST, ATTREX and CONTRAST," *Atmos. Meas. Tech.*, vol. 9, pp. 5213–5225, 2016.

[5] J. M. St. Clair, A. K. Swanson, S. A. Bailey, and T. F. Hanisco, "CAFE: a new, improved non-resonant laser-induced fluorescence instrument for airborne in situ measurement of formaldehyde," *Atmos. Meas. Tech.*, vol. 12, no. 8, pp. 4581–4590, 2019.

[6] J. M. St. Clair, A. K. Swanson, S. A. Bailey, G. M. Wolfe, J. E. Marrero, L. T. Iraci, J. G. Hagopian, and T. F. Hanisco, "A new non-resonant laser-induced fluorescence instrument for the airborne in situ measurement of formaldehyde," *Atmos. Meas. Tech.*, vol. 10, no. 12, pp. 4833–4844, 2017.

[7] M. R. Sargent, D. S. Sayres, J. B. Smith, M. Witinski, N. T. Allen, J. N. Demusz, M. Rivero, C. Tuozzolo, and J. G. Anderson, "A new direct absorption tunable diode laser spectrometer for high precision measurement of water vapor in the upper troposphere and lower stratosphere," *REVIEW OF SCIENTIFIC INSTRUMENTS*, vol. 84, JUL 2013.

[8] R. A. Washenfelder, A. O. Langford, H. Fuchs, and S. S. Brown, "Measurement of glyoxal using an incoherent broadband cavity enhanced absorption spectrometer," *Atmos. Chem. Phys.*, vol. 24, no. 8, pp. 7779–7793, 2008.

[9] A. Bucholtz, "Rayleigh-scattering calculations for the terrestrial atmosphere," *Appl. Opt.*, vol. 15, no. 34, p. 2765, 1995.

[10] V. Gorshelev, A. Serdyuchenko, M. Weber, W. Chehade, and J. P. Burrows, "High spectral resolution ozone absorption cross-sections amp;ndash; part 1: Measurements, data analysis and comparison with previous measurements around 293 k," *Atmos. Meas. Tech.*, vol. 2, no. 7, pp. 609–624, 2014.

[11] R. A. Hannun, A. K. Swanson, S. A. Bailey, T. F. Hanisco, T. P. Bui, I. Bourgeois, J. Peischl, and T. B. Ryerson, "A cavity-enhanced ultraviolet absorption instrument for high-precision,

fast-time-response ozone measurements," *Atmos. Meas. Tech.*, vol. 12, no. 13, pp. 6877–6887, 2020.

[12] E. R. Crosson, "A cavity ring-down analyzer for measurements of atmospheric levels of methane, carbon dioxide, and water vapor," *Appl. Phys. B*, vol. 92, pp. 403–408, 2008.

[13] E. M. Weinstock, E. J. Hintsa, A. E. Dessler, J. F. Oliver, N. L. Hazen, J. N. Demusz, N. T. Allen, L. B. Lapson, and J. G. Anderson, "New fast-response photofragment fluorescence hygrometer for use on the nasa er-2 and the perseus remotely piloted aircraft," *Review Of Scientific Instruments*, vol. 65, pp. 3544–3554, 1994.

[14] E. J. Hintsa, E. M. Weinstock, J. G. Anderson, and R. D. May, "On the accuracy of in situ water vapor measurements in the troposphere and lower stratosphere with the harvard lyman-α hygrometer,," *Journal of Geophysical Research*, vol. 104, pp. 183–8189,, 1999.

[15] E. M. Weinstock, J. B. Smith, D. S. Sayres, J. V. Pittman, J. R. Spackman, E. J. Hintsa, T. F. Hanisco, E. J. Moyer, J. M. St Clair, M. R. Sargent, and J. G. Anderson, "Validation of the harvard lyman-alpha in situ water vapor instrument: Implications for the mechanisms that control stratospheric water vapor," *JOURNAL OF GEOPHYSICAL RESEARCH-ATMOSPHERES*, vol. 114, DEC 2 2009.

[16] J. B. Smith, *The Sources and Significance of Stratospheric Water Vapor: Mechanistic Studies from Equator to Pole*. PhD thesis, Harvard University, Dept. of Earth and Planetary Sciences, 2012.

[17] D. S. Sayres, E. J. Moyer, T. F. Hanisco, J. M. Clair, F. N. Keutsch, A. O'Brien, N. T. Allen, L. Lapson, J. N. Demusz, M. Rivero, T. Martin, M. Greenberg, C. Tuozzolo, G. S. Engel, J. H. Kroll, J. B. Paul, and J. G. Anderson, "A new cavity based absorption instrument for detection of water isotopologues in the upper troposphere and lower stratosphere," *Review Of Scientific Instruments*, vol. 80, 2009.

[18] R. S. Gao, H. Telg, R. J. McLaughlin, S. J. Ciciora, L. A. Watts, M. S. Richardson, J. P. Schwarz, A. E. Perring, T. D. Thornberry, A. W. Rollins, M. Z. Markovic, T. S. Bates, J. E. Johnson, and D. W. Fahey, "A light-weight, high-sensitivity particle spectrometer for PM2.5 aerosol measurements," *Aerosol Science and Technology*, vol. 50, no. 1, pp. 88–99, 2016.

[19] K. P. Bowman and C. R. Homeyer, "GridRad - Three-Dimensional Gridded NEXRAD WSR-88D Radar Data," 2017.

[20] C. R. Homeyer, "Formation of the enhanced-v infrared cloud top feature from high-resolution three-dimensional radar observations," *J. Atmos. Sci.*, vol. 71, pp. 332–348, 2014.

[21] C. R. Homeyer and K. P. Bowman, "Algorithm description document for version 3.1 of the three-dimensional gridded nexrad wsr-88d radar (gridrad) dataset," tech. rep., available online at http://gridrad.org, 2017.

[22] J. W. Cooney, K. P. Bowman, C. R. Homeyer, and T. M. Fenske, "Ten-year analysis of tropopause-overshooting convection using gridrad data," *J. Geophys. Res. Atmos.*, vol. 123, pp. 329–343, 2018.

[23] OFCM, "Federal Meterological Handbook No. 11 – Doppler Radar Meteorological Observations, Part B: Doppler Radar Theory and Meteorology." FCM-H11B-2005 (Available online at http://www.ofcm.gov/publications/fmh/allfmh2.htm), 2005.

[24] OFCM, "Federal Meterological Handbook No. 11 – Doppler Radar Meteorological Observations, Part C: WSR-88D Products and Algorithms." FCM-H11C-2006 (Available online at http://www.ofcm.gov/publications/fmh/allfmh2.htm), 2006.

[25] J. W. Cooney, K. M. Bedka, K. P. Bowman, K. V. Khlopenkov, and K. Itterly, "Comparing

tropopause-penetrating convection identifications derived from NEXRAD and GOES over the contiguous united states," *J. Geophys. Res. Atmos.*, vol. 126, p. e2020JD034319, 2021.

[26] K. V. Khlopenkov, K. M. Bedka, J. W. Cooney, and K. Itterly, "Recent advances in detection of overshooting cloud tops from longwave infrared satellite imagery," *J. Geophys. Res. Atmos.*, vol. 126, p. e2020JD0344359, 2021.

[27] K. P. Bowman, "Large-scale isentropic mixing properties of the Antarctic polar vortex from analyzed winds," *J. Geophys. Res.*, vol. 98, no. D12, pp. 23,013–23,027, 1993.

[28] K. P. Bowman and G. D. Carrie, "The mean-meridional transport circulation of the troposphere in an idealized GCM," *J. Atmos. Sci.*, vol. 59, pp. 1502–1514, 2002.

[29] K. P. Bowman, J. C. Lin, A. Stohl, R. Draxler, P. Konopka, A. Andrews, and D. Brunner, "Input data requirements for Lagrangian trajectory models," *Bull. Amer. Meteorol. Soc.*, vol. 94, pp. 1051–1058, 2013.

[30] W. C. Skamarock, J. B. Klemp, J. Dudhia, D. O. Gill, D. M. Barker, M. G. Duda, X.-Y. Huang, W. Wang, and J. G. Powers, "A description of the Advanced Research WRF version 3," NCAR Tech. Note 475+STR, 2008.

[31] G. A. Grell, S. E. Peckham, R. Schmitz, S. A. McKeen, G. Frost, W. C. Skamarock, and B. Eder, "Fully coupled "online" chemistry within the WRF model," *Atmos. Environ.*, vol. 39, pp. 6957–6975, 2005.

[32] J. D. Fast, W. I. Gustafson Jr., R. C. Easter, R. A. Zaveri, J. C. Barnard, E. G. Chapman, G. A. Grell, and S. E. Peckham, "Evolution of ozone, particulates, and aerosol direct radiative forcing in the vicinity of houston using a fully coupled meteorology-chemistry-aerosol model," *Journal of Geophysical Research: Atmospheres*, vol. 111, no. D21, 2006.

[33] C. R. Homeyer, "Numerical simulations of extratropical tropopause-penetrating convection: Sensitivities to grid resolution," *J. Geophys. Res. Atmos.*, vol. 120, pp. 7174–7188, 2015.

[34] D. B. Phoenix, C. R. Homeyer, and M. C. Barth, "Sensitivity of simulated convection-driven stratosphere-troposphere exchange in WRF-Chem to the choice of physical and chemical parameterization," *Earth and Space Science*, vol. 4, 2017.

[35] L. K. Emmons, S. Walters, P. G. Hess, J.-F. Lamarque, G. G. Pfister, D. Fillmore, C. Granier, A. Guenther, D. Kinnison, T. Laepple, J. Orlando, X. Tie, G. Tyndall, C. Wiedinmyer, S. L. Baughcum, and S. Kloster, "Description and evaluation of the model for ozone and related chemical tracers, version 4 (mozart-4)," *Geoscientific Model Development*, vol. 3, no. 1, pp. 43–67, 2010.

[36] E. R. Mansell, C. L. Ziegler, and E. C. Bruning, "Simulated electrification of a small thunderstorm with two-moment bulk microphysics," *J. Atmos. Sci.*, vol. 67, pp. 171–194, 2010.

[37] S.-Y. Hong, Y. Noh, and J. Dudhia, "A new vertical diffusion package with an explicit treatment of entrainment processes," *Mon. Wea. Rev.*, vol. 134, pp. 2318–2341, 2006.

[38] W. R. Stockwell, F. Kirchner, M. Kuhn, and S. Seefeld, "A new mechanism for regional atmospheric chemistry modeling," *Journal of Geophysical Research: Atmospheres*, vol. 102, no. D22, pp. 25847–25879, 1997.

[39] R. Ahmadov, S. A. McKeen, A. L. Robinson, R. Bahreini, A. M. Middlebrook, J. A. de Gouw, J. Meagher, E.-Y. Hsie, E. Edgerton, S. Shaw, and M. Trainer, "A volatility basis set model for summertime secondary organic aerosols over the eastern united states in 2006," *Journal of Geophysical Research: Atmospheres*, vol. 117, no. D6, 2012.

[40] I. J. Ackermann, H. Hass, M. Memmesheimer, A. Ebel, F. S. Binkowski, and U. Shankar, "Modal aerosol dynamics model for europe: development and first applications," *Atmo-*

spheric Environment, vol. 32, no. 17, pp. 2981 – 2999, 1998.

[41] B. Schell, I. J. Ackermann, H. Hass, F. S. Binkowski, and A. Ebel, "Modeling the formation of secondary organic aerosol within a comprehensive air quality model system," *Journal of Geophysical Research: Atmospheres*, vol. 106, no. D22, pp. 28275–28293, 2001.

[42] M. J. Iacono, J. S. Delamere, E. J. Mlawer, M. W. Shephard, S. A. Clough, and W. D. Collins, "Radiative forcing by long-lived greenhouse gases: Calculations with the AER radiative transfer models," *J. Geophys. Res.*, vol. 113, p. D13103, 2008.

[43] A. Guenther, T. Karl, P. Harley, C. Wiedinmyer, P. I. Palmer, and C. Geron, "Estimates of global terrestrial isoprene emissions using megan (model of emissions of gases and aerosols from nature)," *Atmospheric Chemistry and Physics*, vol. 6, no. 11, pp. 3181–3210, 2006.

[44] O. Wild, X. Zhu, and M. J. Prather, "Fast-j: Accurate simulation of in- and below-cloud photolysis in tropospheric chemical models," *Journal of Atmospheric Chemistry*, vol. 37, pp. 245–282, Nov 2000.

[45] R. J. Salawitch, S. C. Wofsy, P. O. Wennberg, R. C. Cohen, J. G. Anderson, D. W. Fahey, R. S. Gao, E. R. Keim, E. L. Woodbridge, R. M. Stimpfle, J. P. Koplow, D. W. Kohn, C. R. Webster, R. D. May, L. Pfister, E. W. Gottlieb, H. A. Michelsen, G. K. Yue, J. C. Wilson, C. A. Brock, H. H. Jonsson, J. E. Dye, D. Baumgardner, M. H. Proffitt, M. Loewenstein, J. R. Podolske, J. W. Elkins, G. S. Dutton, E. J. Hintsa, A. E. Dessler, E. M. Weinstock, K. K. Kelly, K. A. Boering, B. C. Daube, K. R. Chan, and S. W. Bowen, "The distribution of hydrogen, nitrogen, and chlorine radicals in the lower stratosphere: implications for changes in O3 due to emission of NOy from supersonic aircraft," *Geophys. Res. Lett.*, vol. 21, pp. 2543–2546, 1994.

[46] L. A. Del Negro, D. W. Fahey, R. S. Gao, S. G. Donnelly, E. R. Keim, J. A. Neuman, R. C. Cohen, K. K. Perkins, L. C. Koch, R. J. Salawitch, S. A. Lloyd, M. H. Proffitt, J. J. Margitan, R. M. Stimpfle, G. P. Bonne, P. B. Voss, P. O. Wennberg, C. T. McElroy, W. H. Swartz, T. L. Kusterer, D. E. Anderson, L. R. Lait, and T. P. Bui, "Comparison of modeled and observed values of NO2 and JNO2 during the POLARIS mission," *J. Geophys. Res.*, vol. 104, pp. 26,687–26,703, 1999.

[47] R. S. Gao, L. A. Del Negro, W. H. Swartz, R. J. Salawitch, S. A. Lloyd, M. H. Proffitt, D. W. Fahey, S. G. Donnelly, J. A. Neuman, R. M. Stimpfle, and T. P. Bui, "JNO2 and high solar zenith angles in the lower stratosphere," *Geophys. Res. Lett.*, vol. 28, pp. 2405–2408, 2001.

[48] R. M. Stimpfle, D. M. Wilmouth, R. J. Salawitch, J. G. Anderson, and T. P. Bui, "First measurements of ClOOCl in the stratosphere: The coupling of ClOOCl and ClO in the arctic polar vortex," *J. Geophys. Res.*, vol. 109, p. D03301, 2004.

[49] R. J. Salawitch, S. C. Wofsy, P. O. Wennberg, R. C. Cohen, J. G. Anderson, D. W. Fahey, R. S. Gao, E. R. Keim, E. L. Woodbridge, R. M. Stimpfle, J. P. Koplow, D. W. Kohn, C. R. Webster, R. D. May, L. Pfister, E. W. Gottlieb, H. A. Michelsen, G. K. Yue, M. J. Prather, J. C. Wilson, C. A. Brock, H. H. Jonsson, J. E. Dye, D. Baumgardner, M. H. Proffitt, M. Loewenstein, J. R. Podolske, J. W. Elkins, G. S. Dutton, E. J. Hintsa, A. E. Dessler, E. M. Weinstock, K. K. Kelly, K. A. Boering, B. C. Daube, K. R. Chan, and S. W. Bowen, "The diurnal variation of hydrogen, nitrogen, and chlorine radicals: implications for the heterogeneous production of HNO2," *Geophys. Res. Lett.*, vol. 21, pp. 2547–2550, 1994.

[50] D. Wilmouth, R. M. Stimpfle, J. G. Anderson, J. W. Elkins, D. F. Hurst, R. J. Salawitch, and L. R. Lait, "Evolution of inorganic chlorine partitioning in the arctic polar vortex," *J. Geophys. Res.*, vol. 111, p. D16308, 2006.

5. Acronyms

ASL	Above Sea Level
ASDC	Atmospheric Sciences Data Center
AWAS	Advanced Whole Air Sampler
CAFE	Compact Airborne Formaldehyde Experiment
CANOE	Compact Airborne Nitrogen diOxide Experiment
CH_4	Methane
CH_2O	Formaldehyde
ClO	Chlorine Monoxide
$ClONO_2$	Chlorine Nitrate
CO	Carbon Monoxide
CO_2	Carbon Dioxide
CONUS	Contiguous United States
DCOTSS	Dynamics and Chemistry of the Summer Stratosphere
DFB	Distributed Feedback
DMP	Data Management Plan
EVS-3	Earth Venture Suborbital 3
GC	Gas Chromatograph
GridRad	Gridded NEXRAD WSR-88D Radar
H_2O	Water Vapor
HAL	Harvard Halogens
ROZE	Rapid OZone Experiment
HUPCRS	Harvard University Picarro Cavity Ringdown Spectrometer
HWV	Harvard Water Vapor
LAMS	Laser Ablation Mass Spectrometry
LS	Lower Stratosphere
MMS	Meteorological Measurement Systems
NAMA	North American Monsoon Anticyclone
N_2O	Nitrous Oxide
NEXRAD	Next Generation Weather Radar
NO	Nitrogen Oxide
NO_2	Nitrogen Dioxide
O_3	Ozone
PALMS	Particle Analysis by Laser Mass Spectrometry
PMT	Photomultiplier Tube
POPS	Printed Optical Particle Spectrometer
QA/QC	Quality Assurance and Quality Control
S:N	Signal-to-Noise
SF_6	Sulfur Hexaflouride
SPMS	Single Particle Mass Spectrometer
TDL	Tunable Diode Laser
UCATS	UAS Chromatograph for Atmospheric Trace Species
UTLS	Upper Troposphere and Lower Stratosphere

VIS	Visible
WI–ICOS	Water Isotopologues – Integrated Cavity Output Spectrometer
WS-CRDS	Wavelength-Scanned Cavity Ringdown Spectroscopy
WSR-88D	Weather Surveillance Radar – 1988 Doppler